Measuring the interior of in-use sewage pipes using 3D vision

Bahnsen, Chris H.; Clement, Anders; Larsen, Hans C.Ø.; Moeslund, Thomas B.

Published in:
Automation in Construction

DOI (link to publication from Publisher):
10.1016/j.autcon.2023.104864

Publication date:
2023

Document Version
Publisher's PDF, also known as Version of record

Automation in Construction 151 (2023) 104864

Contents lists available at ScienceDirect

Automation in Construction

journal homepage: www.elsevier.com/locate/autcon

Measuring the interior of in-use sewage pipes using 3D vision

Chris H. Bahnsen *, Anders Clement, Hans C.Ø. Larsen, Thomas B. Moeslund

Visual Analysis and Perception Laboratory, Aalborg University, Rendsburggade 14, Aalborg, 9000, Denmark

ARTICLE INFO

Keywords:
Computer vision
3D vision
Sewage pipes
Diameter estimation
Human-in-the-loop

ABSTRACT

Sewage pipes may be renovated using tailored linings. However, the interior diameter of the pipes must be measured prior to renovation. This paper investigates the use of 3D vision sensors for measuring the interior diameter of sewage pipes, removing the need for human entry in the pipes. The 3D sensors are residing in a waterproof box that is lowered into the well. A RANSAC-based method is used for cylinder estimation from the acquired point clouds of the pipe and the diameter of these cylinders is used as a measure of the interior pipe diameter. The method is tested in 74 real-world sewage pipes with diameters between 150- and 1100 mm. The diameter of 68 pipes is measured within a tolerance of ±20 mm whereas 8 pipes are above. It was found that the faulty estimates can be detected in the field using a combination of human-in-the-loop qualitative and quantitative data-driven measures.

1. Introduction

Most of the sewage infrastructures are buried under other infrastructures such as roads and pathways. As a consequence, the vastness and complexities of a sewage network is often overlooked in daily lives — unless it breaks down.

Across the world, there is a need to continuously renew and replace existing networks of sewage pipes to maintain their functionality. In the United States, a congress report estimates that $271 billion is needed for renewals and replacement of sewage pipes between 2012 to 2037 [1]. A 2021 report [2] estimated that approximately $3 billion is spent in a single year on replacement and repairs of 7,551 km of wastewater pipes. In Germany, the extent of the sewage network is 594,000 km [3] and more than 11% of the network was built before 1960 [3]. Approximately 1% of the German sewage network is renewed each year [4].

There are two main methods for renewal of sewage pipes: replacement or renovation. A complete replacement of the old sewage pipe requires an excavation of the road above, creating costly interruptions of the traffic and generating noise and nuisances to the neighbors. To avoid a costly replacement, the sewage network may instead be refurbished by inserting a cured-in-place-pipe (CIPP) lining into the existing pipe. The CIPP technique may extend the service life of the pipe by up to 50 years [5–7]. However, the CIPP lining must be tailored to the exact dimensions of the host pipe. Otherwise, there is a risk of wrinkles or folds in the final lining, reducing the capacity of the renovated pipe and increasing the risk that objects get stuck in the pipe [8]. A high occurrence of wrinkles in the final lining will decrease the strength of the renovated pipe and may obstruct subsequent inspection by CCTV vehicles [9]. A faulty CIPP lining may be repaired but the process is costly [8]. It is therefore necessary to know the exact dimensions of the pipe in question for renovation. Unfortunately, one cannot assume that existing maps of sewage networks are accurate; the contractor might have used other pipes than agreed upon and record management errors and digitization errors might have occurred since the network was built.

The current method of assessing the diameter of the pipe is by manual inspection; a worker climbs to the bottom of a manhole to measure the interior diameter of the pipe. However, this is an unhealthy and unsafe work environment due to the toxic gasses present in the sewage pipe. For safety concerns, the measurement process must be supervised above-ground by another worker who can facilitate an evacuation process if necessary. The health and safety risks imposed by the current measurement method calls for an alternative approach that does not require the entrance of humans in manholes.

2. Contribution

This work investigates how to obtain reliable measurements of the interior diameter of in-use sewage pipes by the use of off-the-shelf 3D cameras and hardware. A RANdom SAmple Consensus (RANSAC)-based approach is used to model a cylinder from the point clouds acquired from the 3D cameras. The diameter of the estimated cylinder is used as an estimator for the interior diameter of the investigated sewage pipe. An overview of the proposed method is found in Fig. 1. Once fully

* Corresponding author.
E-mail address: cb@create.aau.dk (C.H. Bahnsen).

https://doi.org/10.1016/j.autcon.2023.104864
Received 29 August 2022; Received in revised form 24 March 2023; Accepted 1 April 2023
Available online 12 April 2023

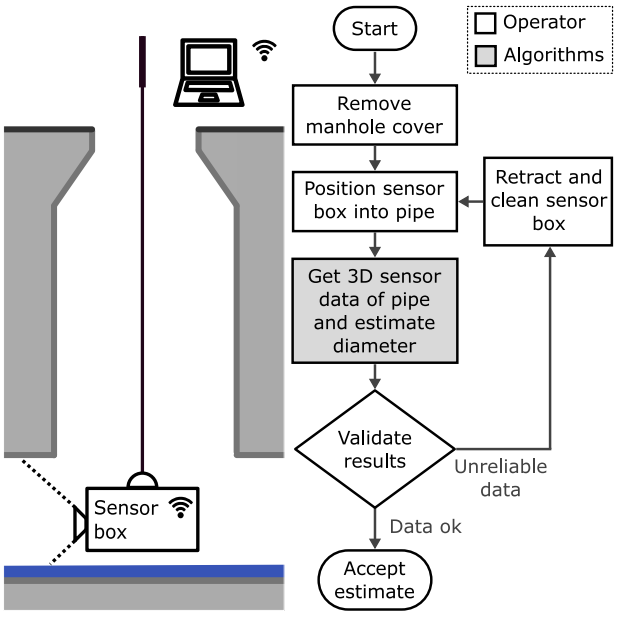

(a) Physical setup (b) Overall workflow

Fig. 1. Overview of the proposed method for 3D vision-based measurement of sewage pipes. 3D cameras inside a waterproof box are lowered into the well to estimate the interior diameter of the pipe.

matured, the proposed method will eliminate the need for human entry in the well to measure the diameter, significantly improving the work environment. Whereas the current measurement method requires two workers to carry out the measurement process, only a single worker is required for the proposed method, enabling cost savings for utility companies.

The overall contributions are:

- The proposed method is the first to show the applicability of using off-the-shelf 3D sensors to measure the diameter of multiple in-use sewage pipes.
- Within the domain of sewer pipe measurements, this paper suggests a novel human-in-the-loop approach for iterative improvement and verification of measurements.

Our specific contributions are summarized as follows:

- Using off-the-shelf hardware, a prototype is constructed that can be inserted into operational sewage pipes and acquire a series of 3D images of the pipes.
- The prototype and method are tested in a multitude of different real life scenarios. Concretely, data from 74 different, in-use sanitary sewer and storm drainage pipes are used. Results show that the method can estimate the diameter of the pipe within a margin of ±20 mm.
- It is shown that both data-driven quantitative and human-in-the-loop qualitative methods can successfully filter out incorrect data and unreliable estimates.

3. Related work

In the following section, related work within interior measurement and profiling of pipes is highlighted. References to works within sewer defect inspection and structural condition assessment [10] are not listed, as it is the overall metric geometry of the pipe that is the focus of the paper, not the structural condition.

3.1. Laser-based interior profiling

Pioneers Kämpfer et al. [11] combined a traditional CCTV-camera with a laser beam attached to a mirror that enabled an operator to measure the cross-section of the pipe as well as reconstruct the pipe profile in 3D. The authors report a maximum estimation error of ±1% in metal pipes. A vastly upgraded laser scanner is demonstrated in [12] that achieves sub-millimeter reconstruction accuracy on the investigated laboratory pipe. Similar setups using a rotating ring beam device and a camera is shown in [13–16]. A physical robot with a dual-ring laser profiler is prototyped in [17,18], showing an average pipe reconstruction error of 0.4 mm and 1.5 mm, respectively. In the KANTARO robot [19], a single laser profiler is combined with a stereo camera to jointly capture profile and depth information. The set-up provides detection of manholes and joints but the paper does not report the accuracy of the reconstructed interior profile.

Stanić et al. [20] equip a CCTV inspection vehicle with a laser profiler and a custom-built back plate to be used for measurement of the distance traveled. By carefully designing and calibrating the cameras and lenses, the authors achieved a maximum reconstruction error of 1.8 mm in a old sewer pipe. However, it is not straightforward to transfer the setup of [20] to in-use sewers.

In general, laser profiling techniques generate an accurate reconstruction of the pipe. The technique requires that the laser beam is located inside the investigated pipe and that the position of the laser and camera may be stabilized to avoid shaking. The stabilization requirement also applies for camera-based reconstruction techniques.

3.2. Camera-based reconstruction

The related work within camera-based reconstruction is divided into three sections: monocular approaches using either equidistant, fish-eye lenses or conventional pin-hole cameras alongside approaches using one or more depth cameras.

3.2.1. Fish-eye camera

A fish-eye, or equidistant, camera is used in [21] to construct a point cloud of a sewer pipe. Corresponding point pairs from epipolar geometry are used as input to a circle fitting algorithm that created a tubular model of the traversed pipe. Zhang et al. [22] acquire a 3D pipe model from fisheye images of a sewer pipe partially filled with water. As with other methods only relying on monocular cameras [21], the scale of the reconstruction is unknown.

Esquivel et al. [23,24] use an industry-grade, rugged fish-eye camera (IBAK Panorama) to create a dense reconstruction of a sewer well. The camera is lowered into the well from above, taking images every 50 mm of the travel. Feature-tracking is performed on the unrolled fish-eye images and structure from motion is applied to produce an initial reconstruction. The scale of the reconstruction is determined by the length of the line lowering the camera into the sewer well. The acquired point cloud is divided into sections in order to estimate the cross-sectional profile of the sewer well. By assuming either a rectangular or a elliptical profile of the cross-section, the authors estimate the true metric profile of the sewer well with an average error of 1%–2%.

3.2.2. Conventional camera

Kolesnik and Baratoff [25,26] use a Hough transform to extract circles from monocular images as the robot drives through the sewer pipe. The distance traveled by the robot can be estimated by knowing the interior diameter of the pipe.

A multi-view association of SIFT features is used in [27] to construct a sparse depth map for partial reconstruction of a large-diameter underground tunnel. The cylindrical constraint is used for estimating a subsection of the interior surface of the tunnel. The method looks promising, but the results are only evaluated qualitatively.

Kagami et al. [28] use a monocular endoscopic camera to create a 3D model of the pipe. A classical feature-matching structure-from-motion (SfM) scheme is combined with a customized bundle adjustment method that uses prior knowledge of the conical shape of the pipe. The investigated pipes are reconstructed with a radius error rate between 1%–7%. A similar SfM algorithm is applied in [29] to estimate the diameter of 200 mm–250 mm steel, concrete, and PVC pipes. The estimation accuracy on the steel and concrete pipes is 1.4% and 2.4%, respectively. However, the algorithm is not able to reconstruct a clean PVC pipe due to missing features on the interior.

Dense 3D reconstructions of pipes are performed in [30–33], however, the authors do not report the metric accuracy of the reconstruction.

3.2.3. Depth camera

The use of a MESA SR-3000 Time-of-Flight (ToF) camera for pipe reconstruction is investigated in [34]. The authors fit both cylindrical models and conical models to the acquired point clouds and find the conical models to find suitable matches. The metric accuracy of the fitted models is not reported but the authors do note that the reconstructed point cloud appears larger than the real pipe, possibly due to secondary reflections and lens scattering. The upgraded MESA SR-4000 ToF camera is used in [35] to measure the interior of a sewer pipe in a laboratory environment. A cylinder is estimated from the acquired point cloud using either a RANSAC or a Hough transform. The results show that a RANSAC-based approach is capable of accurately estimating the pose of the camera with respect to the pipe. However, the paper does not report on the accuracy of the cylinder estimation of the pipe.

Bellés and Pla [36] create a setup consisting of two Kinect V1 cameras and a mini-PC that is lowered into the sewer well. The authors report a reconstruction accuracy of 1% for the estimation of the sewer well and 10 mm for the diameter estimation of the inlet pipes. Yoshimoto et al. [37] investigate the use of a stereo endoscopic camera to accurately reconstruct a camera calibration pattern that is inserted into small, clean pipes. Experiments with pipe diameters between 26 mm and 36 mm show reconstruction errors below 1%.

Bahnsen et al. [38] investigated the use of a Realsense D435 active stereo camera and a PMD CamBoard pico flexx ToF camera for creating an accurate point cloud representation of PVC pipes in a laboratory setting and an outdoor test setup. The results showed that the pico flexx created a significantly more accurate point cloud than the Realsense camera, resulting in an average reconstruction error of approximately 20 mm and 75 mm, respectively. The detrimental performance of the Realsense camera is largely due to excessive noise in the point cloud that is located far from the physical pipe.

The accuracy of the pico flexx ToF camera in clean 400 mm PVC pipes was investigated by Haurum et al. [39]. The authors found that the accuracy of the acquired point cloud varied between +20 mm and −60 mm when comparing the ToF camera to a laser range finder.

The findings from the literature show that approaches based on monocular cameras, either conventional or fish-eye, are not capable of estimating a metric reconstruction of the interior profile of the pipe without additional knowledge. Thus, a depth camera is necessary if the goal is an accurate estimate based solely on the output of a single sensor. The investigated literature shows that it is possible to acquire an accurate metric estimate of the interior profile of a pipe under laboratory conditions [35–38]. In this work, it is investigated whether this holds true for in-use sewer pipes as well.

4. Materials and methods

The experiences from [38] is taken as point of departure and it is investigated if the Realsense D435 active stereo camera (Realsense) and PMD CamBoard pico flexx ToF camera (pico flexx) are suitable for estimation of interior pipe diameters in real-world sanitary sewer and storm drainage pipes. In the following, the physical acquisition platform is described followed by the data acquisition process and framework for pipe radius estimation.

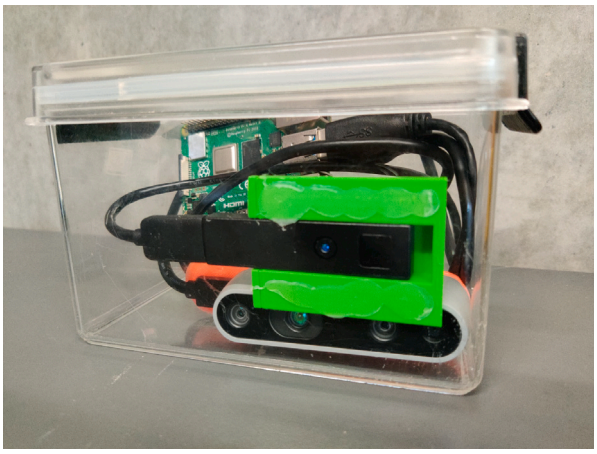

Fig. 2. The sensor and computational hardware fitted inside a waterproof enclosure.

Table 1
List of equipment for the physical recording platform.

PMD Camboard pico flexx
Intel Realsense D435i
Raspberry Pi 4 with 8GB RAM, 128GB SD card
Power bank, 10,000 mAh
Waterproof transparent enclosure
Flashlight
Extendable carbon fiber rod

4.1. Physical platform

Sewers are a hostile environment. The cameras and other electrical components must therefore be fitted inside a waterproof enclosure. In order to make the waterproofing easier, there must be no wiring through the box, e.g. the electronics inside the box must be self-sufficient. This is achieved by connecting the two cameras to a Raspberry Pi that is powered by a standard power bank. The Raspberry Pi creates a stand-alone WiFi hotspot such that it may be controlled from an human operator standing on the ground with a PC. A 3D-printed camera mount is fastened with glue to the side of the box to make sure that the position of the cameras is fixed. The prototype enclosure with sensors is shown in Fig. 2.

In the test sites that are considered for the experiments, the pipes inside the sewer well are located 1–10 m below ground. To safely lower the sensor box into the well and position it into the pipe, the enclosure is fitted to the bottom of an extendable rod. Furthermore, a torch is attached to the bottom of the enclosure to light up the pipe such that the Realsense camera can capture RGB images for human inspection and verification. The full list of materials for the experiments is found in Table 1

4.2. Data acquisition process

At each well, measurements were performed according to the following procedure:

1. Remove the manhole cover to gain access to the well.
2. Assess which pipes are present and correlate this against the pipe map provided by the water utility company.
3. For each pipe inside the well:
   (a) Based on the map, assess pipe material and note the reference diameter.
   (b) Use the extendable rod to lower the sensor box into the well.

(c) Locate the sensor box at the top of the pipe and capture 50 depth frames from each camera.
(d) If the diameter of the pipe is larger than 250 mm, repeat step 3c by locating the box approximately in the middle of the pipe.

Step 3d is done to provide a greater variability of the captured data in larger pipes that can accommodate the sensor box at multiple positions. The capture of multiple frames in step 3c is to explore the stability of the sensor data over time as the cameras may not be perfectly still. The exact value, 50, is based on the hardware constraints of the Raspberry Pi as the raw sensor data is stored in RAM before being written to the slower SSD card.

4.3. Interior diameter estimation

Once the depth images have been acquired by both cameras, the interior diameter of the pipe may be estimated. The depth images are corrected for lens distortion by the OpenCV function `undistortPoints` [40] which utilizes the distortion coefficients provided by the camera manufacturers. The corrected depth images are projected to point clouds using the following equations that are based on the pin-hole camera model:

$$X = Z\frac{x' - c_x}{f_x} \tag{1}$$

$$Y = Z\frac{y' - c_y}{f_y} \tag{2}$$

where Z is the metric depth value at position (x', y') in the corrected depth image, X and Y are the corresponding metric positions in the point cloud, and c_x, c_y, f_x, f_y are the principal point offsets and focal lengths in the x and y directions, respectively.

The point clouds are filtered such that they only contains points within:

$$-1\ \text{m} \le X \le 1\ \text{m} \tag{3}$$

$$-1\ \text{m} \le Y \le 1\ \text{m} \tag{4}$$

$$0\ \text{m} < Z \le 5\ \text{m} \tag{5}$$

Since the maximum diameter of the investigated pipes is 1100 mm, these values allow for a margin of error with respect to the positioning of the sensor box. After the filtering, RANSAC will be used to fit a cylinder to each point as described in Algorithm 1 [41]. PROSAC [42] was tried as an alternative but did not result in better performance than RANSAC. The fitted cylinder is described as a point of origin, $\boldsymbol{p}^*$, a direction vector for its main axis, $\vec{\boldsymbol{a}}$, and its radius, r, as illustrated in Fig. 3.

A point is considered an inlier if the minimum distance to the fitted cylinder is less than the RANSAC inlier threshold, $d_{\max}$. As found by Tran et al. [43], the distance from a point, $\boldsymbol{p}_i$, to the cylinder, c, can be calculated as follows:

$$\text{distance}\left(\boldsymbol{p}_i, \text{c}\right) = \left\| \overrightarrow{\boldsymbol{p}_i - \boldsymbol{p}^*} - \left(\overrightarrow{\boldsymbol{p}_i - \boldsymbol{p}^*} \cdot \vec{\boldsymbol{a}}\right)\vec{\boldsymbol{a}} \right\| - r \tag{6}$$

where $\boldsymbol{p}_i$ is point i in the point cloud, $\boldsymbol{p}^*$ is a point on the cylinder's main axis, $\vec{\boldsymbol{a}}$ is a normalized direction vector for the cylinder's axis, and r is the radius of the cylinder. The mean squared error (MSE) of the estimated cylinder is calculated as follows [43]:

$$\epsilon_{\text{MSE}} = \frac{1}{N}\sum_{i=1}^{N} \text{distance}\left(\boldsymbol{p}_i, \text{c}\right) \tag{7}$$

where $\text{distance}\left(\boldsymbol{p}_i, \text{c}\right)$ is defined by Eq. (6). A cylinder is fitted for every depth frame acquired by the pico flexx and Realsense cameras, resulting in a total of 100 cylinder-based diameter estimates per recording conducted in Step 3c of the data acquisition process. In the Experimental results, it is discussed how to combine the estimates into a single diameter estimate for each pipe.

Data: Point cloud, $\mathcal{P}$
Result: Parameters $\{\boldsymbol{p}^*, \vec{\boldsymbol{a}}, r\}$ of fitted cylinder, number of inlier points $\{m\}$, error $\{\epsilon_{\text{MSE}}\}$.
$k \leftarrow 10000$;
$r_{\min} \leftarrow 0.05$;
$r_{\max} \leftarrow 0.6$;
$n \leftarrow 0$;
$m \leftarrow 0$;
1. Keep points in $\mathcal{P}$ within $[0 < z \le 2.5\ \text{m}]$;
2. Estimate normals for each point in $\mathcal{P}$ by using KDTrees with 50 nearest neighbors;
for $d_{\max} \leftarrow 0.01$ **to** 0.24 **by** 0.01 **do**
  while $n \le k$ **do**
    3. Sample two random points, $\boldsymbol{p}_1, \boldsymbol{p}_2 \in \mathcal{P}$;
    4. Estimate a cylinder such that $\vec{\boldsymbol{a}} \perp \boldsymbol{p}_1$, $\vec{\boldsymbol{a}} \perp \boldsymbol{p}_2$, and $r_{\min} < r \le r_{\max}$;
    5. $m_{\text{temp}} \leftarrow \sum_{p \in \mathcal{P}} [\text{distance}\,(\boldsymbol{p}, \text{c}) < d_{\max}]$;
    if $m_{\text{temp}} > m$ **then**
      6. $m \leftarrow m_{\text{temp}}$;
      7. Save current $\{\boldsymbol{p}^*, \vec{\boldsymbol{a}}, r\}$;
      8. Calculate the error, ϵ_{MSE}, according to Eq. (7);
    end
    9. $n \leftarrow n + 1$;
  end
  10. Select the cylinder corresponding to the highest m as the best estimate, save $\{m, \boldsymbol{p}^*, \vec{\boldsymbol{a}}, r, \epsilon_{\text{MSE}}, d_{\max}\}$;
end

Algorithm 1: Procedure for RANSAC-based cylinder estimation from point clouds [41].

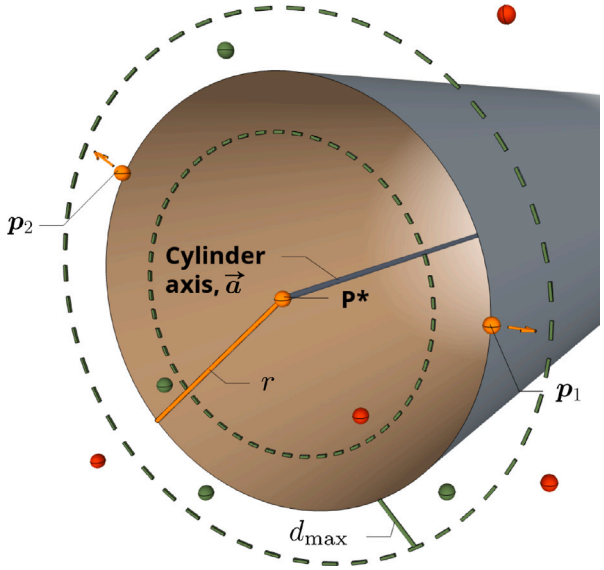

Fig. 3. The cylinder is estimated such that the perimeter of the cylinder touches the randomly selected points $\boldsymbol{p}_1, \boldsymbol{p}_2$ and that the axis of the cylinder is orthogonal to the estimated normals of $\boldsymbol{p}_1, \boldsymbol{p}_2$. The inliers are the points that lie within $d_{\max}$ of the estimated cylinder.

4.4. Allowed tolerance

As mentioned in the Introduction, the estimated interior diameter of the pipe is ultimately used for tailoring a CIPP lining to the investigated pipe. If the diameter of the lining does not correspond to the host pipe, there is a risk of wrinkles or folds in the pipe, reducing throughput and degrading the quality of the refurbished pipe. As a consequence, the

(a) Above-ground (b) Below-ground

Fig. 4. Snapshots from the data acquisition process. One operator positions the box inside the sewer well whereas another operator controls the sensor box using a wireless connection to a PC.

allowable margin of error on the estimated diameter is small; but how small exactly?

A point of departure can be found in the industry standard for pipework components, ISO 6708:1995 [44], that outlines a series of preferred values for the nominal size (DN) of pipework components. The sensor enclosure is designed to fit in pipes with an interior diameter of 150 mm, which corresponds to a preferred ISO value of DN 150. From DN 150, the nominal values increase by 50 up to DN 500 and from DN 500 to DN 1600, the nominal values increase by 100. As a consequence, it is reasonable to frame the measurement task as a classification problem between standardized pipe sizes that increase in steps of at least 50 mm. To provide an unambiguous estimate of the pipe class, the measurement error must therefore be lower than 25 mm. To stay on the safe side of this threshold, the allowable margin of error of the diameter measurement is defined as ±20 mm.

5. Experimental results

The experiments follow the iterative data acquisition and validation process illustrated in Fig. 1. According to this process, initial estimates of the interior diameter of the pipe are computed and subsequently the credibility of these estimates are assessed based on further studies of the data.

5.1. Experimental settings

Measurements are performed in a residential area in Tranbjerg, Denmark. Here, each well contains both sanitary sewers and storm drains. In total, 24 concrete sanitary sewer pipes are measured, ranging in interior diameter from 150 mm to 500 mm. Additionally, 50 concrete storm drainage pipes are measured, ranging in inner diameter from 150 mm to 1100 mm. According to step 3d of the data acquisition process, two measurements are conducted in pipes with a diameter greater than 250 mm, resulting in a total of 101 measurements from 74 pipes.

As the pipes are planned for renovation, their interior diameter is previously measured by a human operator who inserts a physical measuring device into the pipes. These measurements are used as the ground truth reference for the interior diameter of the pipes. Photographs from the data acquisition process are found in Fig. 4.

The pico flexx camera is set to retrieve depth within 1 to 4 meters and the Realsense is set at a resolution of 640 × 480 at 30 fps. For the Realsense camera, it is found that lowering the resolution decrease the amount of noise in the point cloud compared to [38].

5.2. Initial results

As mentioned in the previous section, there is a need to establish a single, consensus estimate based on the diameter estimates computed for each of the 50 frames acquired by each camera. In our experiments, the mean or median of the per-frame diameter estimate from Algorithm 1 are compared with the reference diameter value. The inlier-weighted mean (IWM) of the per-frame diameter estimates has been investigated but have produced diminishing results compared to the mean or median. The inlier-weighted mean is computed as follows:

$$\mathrm{IWM} = \frac{\sum_{n=1}^{50} r_n \iota_n}{\sum_{n=1}^{50} r_n} \tag{8}$$

where r_n is the radius of the estimated cylinder for frame n and ι_n is the percentage of points in the point cloud for frame n whose distance to the estimated cylinder do not exceed $d_{\max}$.

The results from both cameras across all recordings are shown in Fig. 5.

From these results, it is seen that the diameter estimates based on the point clouds from the pico flexx are significantly worse than the estimate based on the Realsense data. Within an allowable margin of error of ±20 mm on the diameter, the percentage of correctly classified pipes are peaking at 64% for the pico flexx whereas the accuracy of the Realsense data reaches a maximum of 89%. For the Realsense, this means that 90 diameter estimates are within the ±20 mm threshold whereas 11 estimates are above. The low accuracy of the picoo flexx reflects the experiences of Haurum et al. [45] but are in contrast to the comparison by Bahnsen et al. [38] where the pico flexx produced more accurate point clouds than the Realsense camera. The cause of the discrepancy with [38] may lie in the housing of the cameras. In [38], the cameras are not enclosed whereas in this work, they are located inside a plastic enclosure that may affect the performance of the infrared emitter in the ToF module.

From Fig. 5 it is also seen that the median is slightly better than the mean for producing a consensus estimate amongst the 50 recorded frames. For the diameter estimate based on the pico flexx, the accuracy is inversely proportional to the RANSAC inlier threshold, $d_{\max}$, whereas this effect is less profound on the Realsense-based estimates. It is noticed that the lowest overall estimation error is achieved by taking the median diameter value of the cylinders that are estimated from the Realsense-based point clouds with $d_{\max} = 90$ mm. The remainder of the experiments in this paper are thus based on this configuration. However, setting $d_{\max}$ within the range of 60 mm to 180 mm would also be sensible. The estimation error relative to the reference diameter of the pipe is shown in Fig. 6. There seems to be no clear correlation between the estimation error and pipes with diameters between 150 and 900 mm whereas the proposed solution struggles in the investigated 1100 mm pipes.

However, even in the best configuration, 11% of the estimates have a diameter estimation error larger than 20 mm. This is not acceptable in a use-case where the estimates are being used to tailor linings for CIPP renovation of the pipes. In the following, it is investigated how to detect and filter the faulty measurements based on the human-in-the-loop paradigm.

If the method is deployed in the future, the authors anticipate that the measurements may be carried out by a single human operator that receives real-time feedback from the 3D cameras. If the image, point cloud, or the calculated metrics indicate that the measurement may be inaccurate, the operator can retrieve the sensor enclosure, clean the outside if necessary, and obtain additional recordings from the pipe according to Fig. 1(b).

5.3. Obtaining trustworthy measurements

Two paths are followed to investigate if it is possible to decrease the measurement error by detecting and removing bad data: (1) data-driven estimators and (2) visual inspection. The proposed data acquisition, cylinder estimation, and cylinder verification pipeline is shown in Fig. 7. The contents of the pipeline are explored in the following.

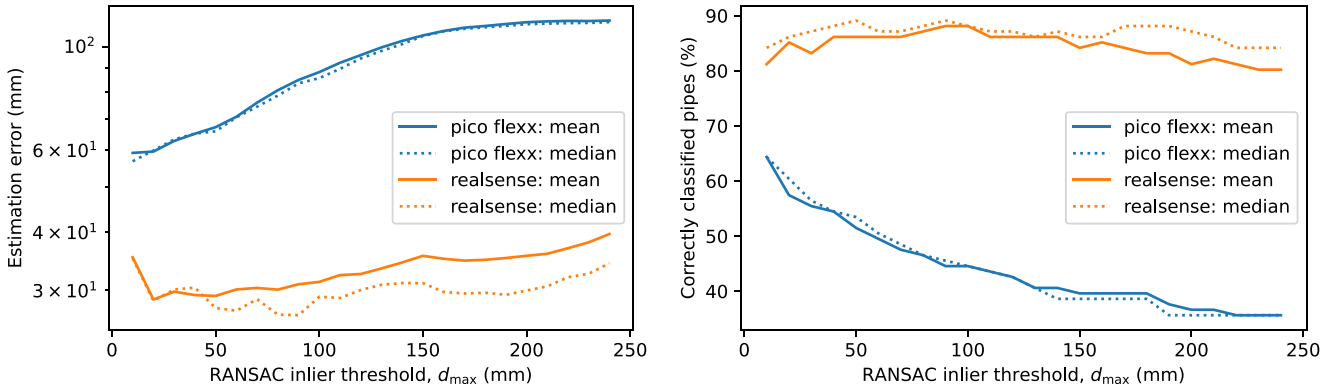

(a) Average diameter estimation error

(b) Percentage of correctly classified pipes within ±20 mm

Fig. 5. Overall diameter estimation performance across cameras and varying RANSAC inlier thresholds, d_{max}. Two approaches are compared for calculating a consensus diameter estimate across a recording of 50 frames; taking the mean or median value. The estimates based on the Realsense depth data fare significantly better than the pico flexx counterparts. The setup with the lowest estimation error is found by taking the median diameter estimate from the point clouds provided by the Realsense camera at $d_{max} = 90$ mm.

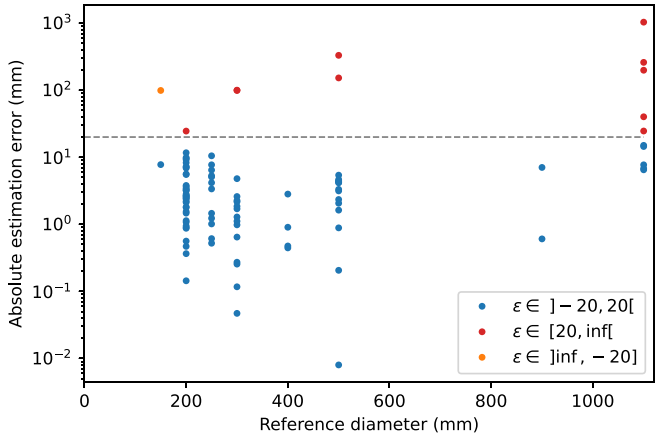

Fig. 6. Diameter estimation error across pipe sizes.

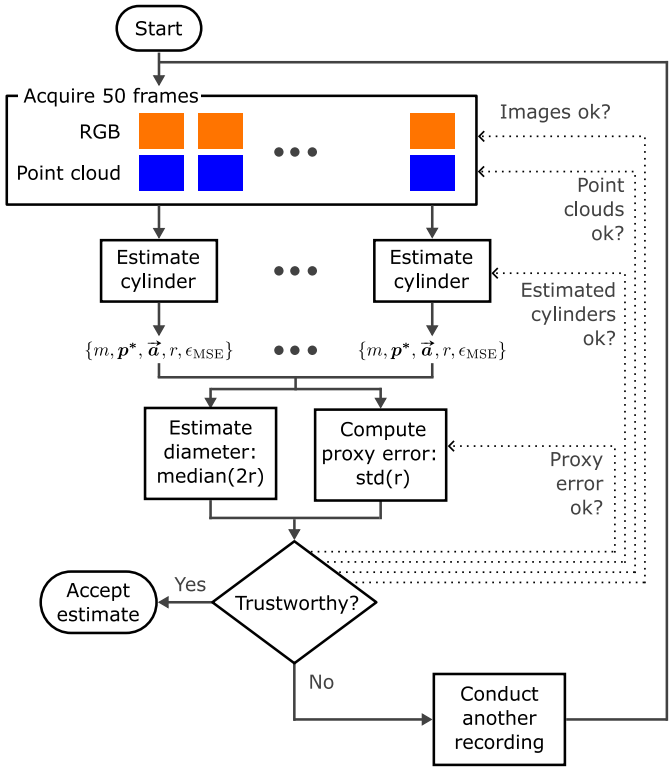

Fig. 7. Overview of the proposed human-in-the-loop data acquisition and verification pipeline.

Data-driven estimators. For the data-driven estimators, the use of basic statistical metrics is investigated in order not to overfit any estimator to the acquired data and to enable real-time calculation of the metrics on embedded hardware. As written in the above, each camera acquires 50 depth frames from each recording. From each of these frames, a cylinder is estimated. The descriptors and error metrics of the estimated cylinder may be used as proxy metrics for the diameter estimation error reported in Fig. 5(a). The mean and standard deviation of the following descriptors are investigated as candidate proxy metrics:

1. Inlier percentage, e.g. the percentage of points in the point cloud whose distance to the estimated cylinder do not exceed d_{max}.
2. Mean-squared error of the estimated cylinder, ϵ_{MSE}.
3. Estimated cylinder radius, r.
4. Cylinder orientation relative to the camera's z-axis.

The median, skewness, and the interquartile range of the descriptors are also investigated but gave diminishing results. The cylinder's orientation relative to the z-axis of the camera is calculated as the cosine similarity [46] between the orientation of the cylinder's axis, $\vec{\boldsymbol{a}}$, and the direction of the z-vector of the camera, $\boldsymbol{z} = (0\,0\,1)$:

$$\text{sim}(\vec{\boldsymbol{a}}, \vec{\boldsymbol{z}}) = \frac{\vec{\boldsymbol{a}} \cdot \vec{\boldsymbol{z}}}{\|\vec{\boldsymbol{a}}\| \cdot \|\vec{\boldsymbol{z}}\|} = \frac{a_z}{\|\vec{\boldsymbol{a}}\|} \tag{9}$$

A linear regression model is fitted to each of the investigated descriptors to assess their feasibility as proxy error metrics. Five-fold cross validation is performed on the data and the average and standard deviation of the F_1-score of the investigated proxy metrics across the five folds are listed in Table 2. The F_1-score is calculated as follows:

$$F_1 = \frac{\text{TP}}{\text{TP} + \frac{1}{2}(\text{FP} + \text{FN})} \tag{10}$$

where TP, FP, and FN are the True Positives, False Positives, and False Negatives classified by the proxy metric, respectively.

From Table 2, it is found that the standard deviation of the estimated radius is the strongest descriptor of the estimated error, followed by the mean value of ϵ_{MSE}. Intuitively, this makes sense; if the standard deviation of the radius estimate is low, the estimated cylinder is stable throughout the 50 acquired depth frames which indicate that the

Table 2
Investigated proxy metrics for the radius estimation error. The (mean, standard deviation) of the F_1-score from the five-fold cross validation of the estimators are listed. The best metric is highlighted in bold. Cyl. orientation is computed according to Eq. (9).

	Mean	Std
% inliers	0.81 (0.14)	0.90 (0.10)
ϵ_{MSE}	0.92 (0.09)	0.91 (0.11)
Radius, r	0.24 (0.32)	**0.95 (0.04)**
Cyl. orientation	0.91 (0.07)	0.91 (0.09)

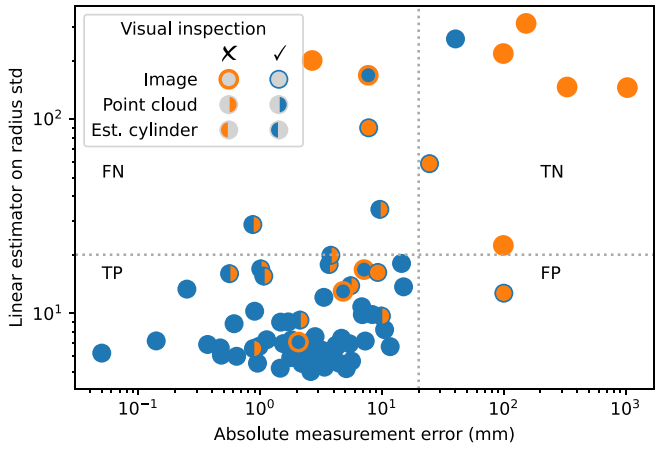

Fig. 8. Using a combination of proxy metrics (radius std) and visual indicators to detect wrong diameter estimates. The color and fill of the circles indicate the qualitative appearance of the image (color of circumference), the quality of the point cloud (right semicircle), and the alignment of the estimated cylinder to the point cloud (left semicircle). The horizontal, dotted line marks the decision threshold of the linear estimator whereas the vertical, dotted line marks the maximum allowable measurement error. TN, FN, TN, and FP are related to the classification by means of the proxy error metric based on radius std.

acquired point clouds are of consistent good quality and are likely to represent the true cylindrical shape of the pipe.

As noted in the description of the data acquisition process, two series of measurements are taken in sufficiently large pipes; however, how to choose one measurement over another? If the radius estimate with the lowest standard deviation is selected, the overall accuracy is 89% with 66 pipes correctly classified and eight pipes classified with an error above 20 mm.

In the following, a combination of visual inspection and the chosen proxy metric is used to filter the remaining bad estimates.

Visual inspection. For the visual inspection task, the quality of the image and the point cloud is assessed based on the following qualitative indicators:

1. Is the image quality reasonable? Is the camera facing the pipe, does the image contain motion blur, etc.
2. Does (part of) the point cloud resemble a cylinder?
3. Does the estimated cylinder align with the point cloud?

The visual quality indicators are of course subjective and based on the experience of the authors with cameras and point clouds. Nonetheless, they may indicate if it is possible to judge the accuracy of the estimate based on the perceived quality of the images and point clouds. The visual quality of every recording is marked in Fig. 8 alongside the chosen proxy metric based on the standard deviation of the radius. A filled blue circle indicates good image quality, a corresponding point cloud that resembles a cylinder, and an estimated cylinder that aligns well with the point cloud. A filled orange circle, on the other hand, indicates that none of these conditions are fulfilled. From Fig. 8, it is seen that cylinders estimated from high-quality images and point clouds (filled blue circles) tend to have lower measurement errors than images and point clouds with lower visual quality (semi-filled orange or filled orange circles).

If the threshold defined from the best fold during cross-validation is used, the proxy error estimate may be used to correctly identify seven bad estimates (TN) whereas five estimates are falsely flagged as erroneous (FN). 61 good estimates are correctly detected (TP) and only one wrong estimate is labeled as 'good' (FP). The threshold is visible from Fig. 8 as a horizontal, dotted gray line.

The classification based on the proxy error estimate can be combined with the visual indicators to get rid of the false positives. For instance, one could choose only to trust good-quality data corresponding to filled blue circles at the cost of additional false negatives. In this context, false positives are several orders of magnitude more severe than false negatives. The cost of a false negative is the cost of conducting another measurement whereas the worst-case cost of a false positive is the cost of removing a tailored inlining from the sewer well. Overall, the results indicate that it is feasible to detect bad estimates in a human-in-the-loop setup that combines visual inspection and data-driven metrics.

Fig. 9 shows samples from six field recordings; two failure-cases (1st and 2nd), a recording with significant motion blur caused by camera motion (3rd), a recording with a decent cylinder estimate despite a noisy point cloud (4th), a successful recording despite water on the lens (5th), and a good estimate of a large sewer pipe (6th).

6. Limitations

Even though the method has been tested in 74 different, real-world sanitary sewer and drainage pipes, the investigated pipes are residing in the same neighborhood which means that the pipes share similarities in terms of age and structural conditions. Since the proposed solution relies on camera system, we are dependent on the reflective properties of the matter residing on the inside of the sewer pipes. This implies that the testing must be expanded to a wider range of structural conditions and different pipe materials, including brick and PVC pipes, to further assess the feasibility of the proposed method,

As seen from Fig. 2, there is significant room for improvement on the design and craftsmanship of the sensor box. A point of departure is the shape of the box; a cylindrical or spherical box would make a better fit to smaller pipes. The water-proofing could be improved and the surface of the box might be coated with a water repellent solution. Furthermore, the linking between the extendable rod and the sensor box would benefit from active stabilization to prevent motion blur.

An important aspect of the pipeline depicted in Fig. 7 is real-time feedback to the human operator that enables the person in question to assess the trustworthiness of the cylinder estimate based on the data-driven and qualitative indicators. Our experience shows that the cylinder estimation on the Raspberry Pi 4 only takes a few seconds which indicate that the main bottleneck may be the wireless transfer of images and point clouds to the operator's computer. However, the operator may study the quality of the first available data and assess the remaining data as it becomes available. Another aspect is the proper training of the operators to assess the quality of the acquired data and the estimated point clouds. It is also open for discussion how to present the data to the operator in a clear, concise, and interpretable manner.

7. Conclusions

This work has explored the feasibility of using 3D cameras for measuring the interior diameter of sewage pipes in the context of producing Cured-In-Place-Piping (CIPP) lining for renovation of the pipes. The Realsense D435i active stereo camera and the PMD CamBoard pico flexx time-of-flight camera are used as representatives of different technologies for 3D sensing. The cameras are placed in a

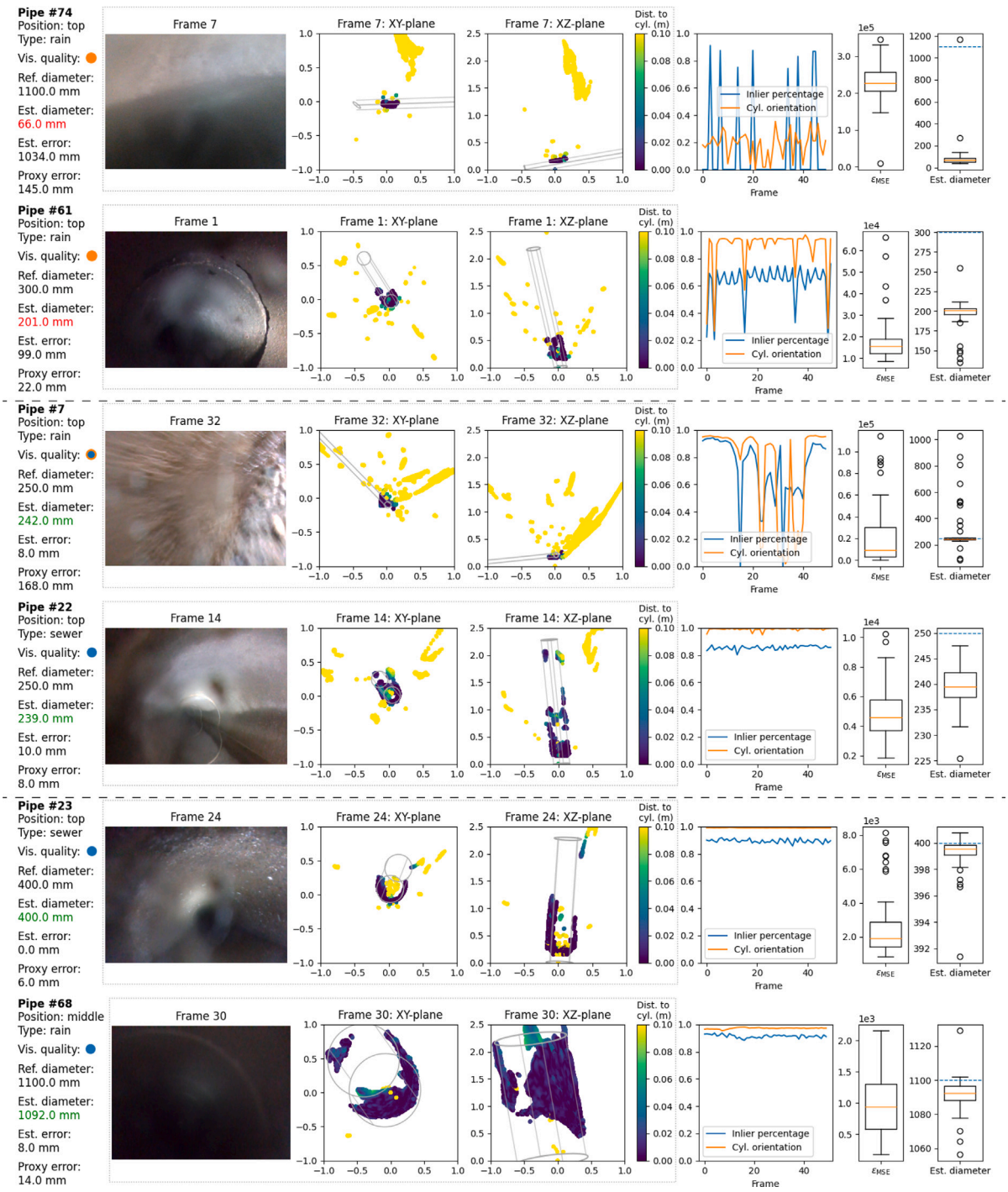

Fig. 9. Samples from six recordings. The RGB image and the point cloud corresponding to a randomly selected frame are visualized within the dotted, gray rectangle. The percentage of inliers and the orientation of the estimated cylinder (Eq. (9)) for the acquired frames are shown to the right of the point clouds. Box plots for ϵ_{MSE} and the diameter of the estimated cylinder are shown in the two columns to the right.

transparent, waterproof box alongside a Raspberry Pi 4, power supply, and additional lighting. An operator uses a extendable rod to lower the box into the well and position it such that the cameras are facing the pipe. Once positioned, the cameras take a series of 3D images of the pipe that are subsequently converted to point clouds. A RANSAC-based algorithm is used for estimating a cylinder from each acquired point cloud. The median diameter of the estimated cylinders is used as the measure of the interior diameter of the pipe.

The proposed method is tested in 74 concrete sanitary sewer and storm drainage pipes located in a Danish suburban neighborhood where the pipes are planned for renovation. In 66 of the investigated 74 pipes, the estimated diameter is correct within a margin of error of ±20 mm whereas eight estimates are above this threshold. It is found that the main cause of the wrong estimates is grounded in bad data and that these data points may be filtered using a combination of qualitative inspection by the human operator and data-driven metrics of the cylinder estimation process. Based on a thorough analysis of the acquired data from testing, it is found that the standard deviation of the estimated radius serves as a good proxy for the diameter estimation error. Combined with qualitative assessment of the acquired images and point clouds and fitness of the estimated cylinder, the operator can filter out the wrong estimates, retract the sensor box for cleaning, and retry.

The proposed review-and-retry process will result in an increase in false negatives, but the cost hereof is conducting another measurement whereas the worst-case expense of a false positive is removing a faulty CIPP lining from the pipe.

Even though the method has been tested in 74 real-world sewage pipes, extended tests are needed in even more pipes to check the real-world applicability of the system under a broader variety of conditions. The results suggest that real-time feedback from the cameras is an important aspect that should be prioritized in a future prototype. Upon further development and maturing, the proposed solution has the potential to eliminate the health risks of the current measurement method and enable cost savings for the companies performing the measurements.

Declaration of competing interest

The authors declare that they have no known competing financial interests or personal relationships that could have appeared to influence the work reported in this paper.

Data availability

Data will be made available on request.

Acknowledgments

This work is supported by Innovation Fund Denmark [grant number 8055-00015A] and is part of the Automated Sewer Inspection Robot (ASIR) project.

References

[1] U. EPA, Clean Watersheds Needs Survey (2012 Report to Congress), Tech. Rep., Office of Transportation and Air Quality, U.S. Environmental Protection Agency (USEPA), Washington, DC, USA, 2012, https://www.epa.gov/sites/default/files/2015-12/documents/cwns_2012_report_to_congress-508-opt.pdf. (Last Accessed on 09 January 2023).

[2] American Society of Civil Engineers (ASCE), 2021 Infrastructure report card - Wastewater, 2021, https://infrastructurereportcard.org/wp-content/uploads/2020/12/Wastewater-2021.pdf. (Last Accessed on 09 January 2023).

[3] Statistisches Bundesamt, Öffentliche wasserversorgung und öffentliche abwasserentsorgung - strukturdaten zur wasserwirtschaft 2016, Tech. Rep., Statistisches Bundesamt, https://www.statistischebibliothek.de/mir/receive/DEHeft_mods_00130296. (Last Accessed on 09 January 2023).

[4] C. Berger, C. Falk, F. Hetzel, J. Pinnekamp, J. Ruppelt, P. Schleiffer, J. Schmitt, Zustand der Kanalisation in Deutschland - Ergebnisse der DWA-Umfrage 2020, Korrespondenz Abwasser, Abfall 67 (12) (2020) 939–953, http://dx.doi.org/10.3242/kae2020.12.001.

[5] A. Jaganathan, E. Allouche, M. Baumert, Experimental and numerical evaluation of the impact of folds on the pressure rating of CIPP liners, Tunnel. Undergr. Space Technol. 22 (5) (2007) 666–678, http://dx.doi.org/10.1016/j.tust.2006.11.007, Trenchless Technology.

[6] V. Kaushal, M. Najafi, Comparative assessment of environmental impacts from open-cut pipeline replacement and trenchless cured-in-place pipe renewal method for sanitary sewers, Infrastructures 5 (6) (2020) 48, http://dx.doi.org/10.3390/infrastructures5060048.

[7] H. Alzraiee, I. Bakry, T. Zayed, Destructive analysis-based testing for cured-in-place pipe, J. Perform. Construct. Facilities 29 (4) (2015) 04014095, http://dx.doi.org/10.1061/(ASCE)CF.1943-5509.0000567.

[8] S. Das, A. Bayat, L. Gay, M. Salimi, J. Matthews, A comprehensive review on the challenges of Cured-In-Place Pipe (CIPP) installations, J. Water Supply: Res. Technol.-Aqua 65 (8) (2016) 583–596, http://dx.doi.org/10.2166/aqua.2016.119.

[9] N. Ampiah, A. Fam, I.D. Moore, Wavy imperfections and the strength of cast-in-place pressure pipe liners, in: Pipelines 2008, 2008, pp. 1–10, http://dx.doi.org/10.1061/40994(321)54.

[10] J.B. Haurum, T.B. Moeslund, A survey on image-based automation of CCTV and SSET sewer inspections, Autom. Constr. 111 (2020) 103061, http://dx.doi.org/10.1016/j.autcon.2019.103061.

[11] W. Kampfer, R. Bartzke, W. Ziehl, Flexible mobile robot system for smart optical pipe inspection, in: W.G. Reuter (Ed.), Nondestructive Evaluation of Utilities and Pipelines II, Vol. 3398, SPIE, International Society for Optics and Photonics, 1998, pp. 75–83, http://dx.doi.org/10.1117/12.302534.

[12] Z. Ma, Y. Hu, J. Huang, X. Zhang, Y. Wang, M. Chen, Q.M. Zhu, A novel design of in pipe robot for inner surface inspection of large size pipes, Mech. Based Des. Struct. Mach. 35 (4) (2007) 447–465, http://dx.doi.org/10.1080/15397730701673296.

[13] T. Wakayama, T. Yoshizawa, Simultaneous measurement of internal and external profiles using a ring beam device, in: Two-and Three-Dimensional Methods for Inspection and Metrology VI, Vol. 7066, International Society for Optics and Photonics, 2008, p. 70660D, http://dx.doi.org/10.1117/12.794388.

[14] W. Jackson, G. Dobie, C. MacLeod, G. West, C. Mineo, L. McDonald, Error analysis and calibration for a novel pipe profiling tool, IEEE Sens. J. 20 (7) (2020) 3545–3555, http://dx.doi.org/10.1109/JSEN.2019.2960939.

[15] P.D.V. Buschinelli, J.R.C. Melo, A.A. Jr., J.M.C. Santos, C.S. Camerini, Optical profilometer using laser based conical triangulation for inspection of inner geometry of corroded pipes in cylindrical coordinates, in: P.H. Lehmann, W. Osten, A. Albertazzi (Eds.), Optical Measurement Systems for Industrial Inspection VIII, Vol. 8788, SPIE, International Society for Optics and Photonics, 2013, p. 87881H, http://dx.doi.org/10.1117/12.2020966.

[16] Z. Liu, D. Krys, The use of laser range finder on a robotic platform for pipe inspection, Mech. Syst. Signal Process. 31 (2012) 246–257, http://dx.doi.org/10.1016/j.ymssp.2012.03.006.

[17] K. Kawasue, T. Komatsu, Shape measurement of a sewer pipe using a mobile robot with computer vision, Int. J. Adv. Robot. Syst. 10 (1) (2013) 52, http://dx.doi.org/10.5772/55261.

[18] X. Chen, F. Zhou, X. Chen, J. Yang, Mobile visual detecting system with a catadioptric vision sensor in pipeline, Optik 193 (2019) 162854, http://dx.doi.org/10.1016/j.ijleo.2019.05.060.

[19] A. Ahrary, M. Ishikawa, Self-localization of autonomous sewer robots by using a stereo camera and a laser scanner, in: 2006 IEEE International Conference on Networking, Sensing and Control, 2006, pp. 78–83, http://dx.doi.org/10.1109/ICNSC.2006.1673121.

[20] N. Stanić, M. Lepot, M. Catieau, J. Langeveld, F.H. Clemens, A technology for sewer pipe inspection (part 1): Design, calibration, corrections and potential application of a laser profiler, Autom. Constr. 75 (2017) 91–107, http://dx.doi.org/10.1016/j.autcon.2016.12.005.

[21] J. Kannala, S.S. Brandt, J. Heikkilä, Measuring and modelling sewer pipes from video, Mach. Vis. Appl. 19 (2) (2008) 73–83, http://dx.doi.org/10.1007/s00138-007-0083-1.

[22] Y. Zhang, R.I. Hartley, J. Mashford, L. Wang, S. Burn, Pipeline reconstruction from fisheye images, J. WSCG 19 (2) (2011) 49–57, https://dblp.org/rec/journals/jwscg/ZhangHMWB11. (Last Accessed at 10 January 2023).

[23] S. Esquivel, R. Koch, H. Rehse, Reconstruction of sewer shaft profiles from fisheye-lens camera images, in: J. Denzler, G. Notni, H. Süße (Eds.), Pattern Recognition, Springer Berlin Heidelberg, Berlin, Heidelberg, 2009, pp. 332–341, http://dx.doi.org/10.1007/978-3-642-03798-6_34.

[24] S. Esquivel, R. Koch, H. Rehse, Time budget evaluation for image-based reconstruction of sewer shafts, in: N. Kehtarnavaz, M.F. Carlsohn (Eds.), Real-Time Image and Video Processing 2010, Vol. 7724, SPIE, International Society for Optics and Photonics, 2010, p. 77240M, http://dx.doi.org/10.1117/12.854538.

[25] M. Kolesnik, G. Baratoff, 3D interpretation of sewer circular structures, in: Proceedings 2000 ICRA. Millennium Conference. IEEE International Conference on Robotics and Automation. Symposia Proceedings (Cat. No.00CH37065), Vol. 2, 2000, pp. 1453–1458, http://dx.doi.org/10.1109/ROBOT.2000.844802.

[26] M. Kolesnik, G. Baratoff, Online distance recovery for a sewer inspection robot, in: Proceedings 15th International Conference on Pattern Recognition, Vol. 1, ICPR-2000, 2000, pp. 504–507, http://dx.doi.org/10.1109/ICPR.2000.905386.

[27] K. Chaiyasarn, T.-K. Kim, F. Viola, R. Cipolla, K. Soga, Image mosaicing via quadric surface estimation with priors for tunnel inspection, in: 2009 16th IEEE International Conference on Image Processing, ICIP, 2009, pp. 537–540, http://dx.doi.org/10.1109/ICIP.2009.5413902.

[28] S. Kagami, H. Taira, N. Miyashita, A. Torii, M. Okutomi, 3D pipe network reconstruction based on structure from motion with incremental conic shape detection and cylindrical constraint, in: 2020 IEEE 29th International Symposium on Industrial Electronics, ISIE, 2020, pp. 1345–1352, http://dx.doi.org/10.1109/ISIE45063.2020.9152377.

[29] S.E. Kahi, D. Asmar, A. Fakih, J. Nieto, E. Nebot, A vison-based system for mapping the inside of a pipe, in: 2011 IEEE International Conference on Robotics and Biomimetics, 2011, pp. 2605–2611, http://dx.doi.org/10.1109/ROBIO.2011.6181697.

[30] A. Reyes-Acosta, I. Lopez-Juarez, R. Osorio-Comparan, G. Lefranc, 3D pipe reconstruction employing video information from mobile robots, Appl. Soft Comput. 75 (2019) 562–574, http://dx.doi.org/10.1016/j.asoc.2018.11.016.

[31] X. Zhang, P. Zhao, Q. Hu, H. Wang, M. Ai, J. Li, A 3D reconstruction pipeline of urban drainage pipes based on MultiviewImage matching using low-cost panoramic video cameras, Water 11 (10) (2019) http://dx.doi.org/10.3390/w11102101, URL https://www.mdpi.com/2073-4441/11/10/2101.

[32] A. Oyama, H. Iida, Y. Ji, K. Umeda, Y. Mano, T. Yasui, T. Nakamura, Three-dimensional mapping of pipeline from inside images using earthworm robot equipped with camera, IFAC-PapersOnLine 52 (22) (2019) 87–90, http://dx.doi.org/10.1016/j.ifacol.2019.11.053, 1st IFAC Workshop on Robot Control WROCO 2019.

[33] R. Zhang, M.H. Evans, R. Worley, S.R. Anderson, L. Mihaylova, Improving SLAM in pipe networks by leveraging cylindrical regularity, in: C. Fox, J. Gao, A. Ghalamzan Esfahani, M. Saaj, M. Hanheide, S. Parsons (Eds.), Towards Autonomous Robotic Systems, Springer International Publishing, Cham, 2021, pp. 56–65, http://dx.doi.org/10.1007/978-3-030-89177-0_6.

[34] J.T. Thielemann, G.M. Breivik, A. Berge, Pipeline landmark detection for autonomous robot navigation using time-of-flight imagery, in: 2008 IEEE Computer Society Conference on Computer Vision and Pattern Recognition Workshops, 2008, pp. 1–7, http://dx.doi.org/10.1109/CVPRW.2008.4563167.

[35] P. Striegl, K. Mönch, W. Reinhardt, Untersuchungen zur Verbesserung der Aufnahmegenauigkeit von Abwasserleitungen, Zfv-Zeitschrift Für Geodäsie, Geoinformation Und Landmanagement (2) (2014) http://dx.doi.org/10.12902/zfv-0013-2014.

[36] C. Bellés, F. Pla*, A kinect-based system for 3D reconstruction of sewer manholes, Comput.-Aided Civ. Infrastruct. Eng. 30 (11) (2015) 906–917, http://dx.doi.org/10.1111/mice.12107.

[37] K. Yoshimoto, K. Watabe, M. Tani, T. Fujinaga, H. Iijima, M. Tsujii, H. Takahashi, T. Takehara, K. Yamada, Three-dimensional panorama image of tubular structure using stereo endoscopy, Int. J. Innovative Comput. Inf. Control 16 (3) (2020) 799–812, http://dx.doi.org/10.24507/ijicic.16.03.799.

[38] C.H. Bahnsen, A.S. Johansen, M.P. Philipsen, J.W. Henriksen, K. Nasrollahi, T.B. Moeslund, 3D sensors for sewer inspection: A quantitative review and analysis, Sensors 21 (7) (2021) http://dx.doi.org/10.3390/s21072553.

[39] J.B. Haurum., M.M.J. Allahham., M.S. Lynge, K.S. Henriksen., I.A. Nikolov., T.B. Moeslund., Sewer defect classification using synthetic point clouds, in: Proceedings of the 16th International Joint Conference on Computer Vision, Imaging and Computer Graphics Theory and Applications - Volume 5: VISAPP, SciTePress, INSTICC, 2021, pp. 891–900, http://dx.doi.org/10.5220/0010207908910900.

[40] G. Bradski, The OpenCV library, 2000, https://www.drdobbs.com/open-source/the-opencv-library/184404319. (Last Accessed on 08 April 2023).

[41] R.B. Rusu, S. Cousins, 3D is here: Point Cloud Library (PCL), in: 2011 IEEE International Conference on Robotics and Automation, 2011, pp. 1–4, http://dx.doi.org/10.1109/ICRA.2011.5980567.

[42] O. Chum, J. Matas, Matching with PROSAC - Progressive sample consensus, in: 2005 IEEE Computer Society Conference on Computer Vision and Pattern Recognition, Vol. 1, CVPR'05, 2005, pp. 220–226, http://dx.doi.org/10.1109/CVPR.2005.221.

[43] T.T. Tran, V.T. Cao, D. Laurendeau, Extraction of cylinders and estimation of their parameters from point clouds, Comput. Graph. 46 (2015) 345–357, http://dx.doi.org/10.1016/J.CAG.2014.09.027.

[44] I. 6708:1995, Pipework Components — Definition and Selection of Dn (Nominal Size), 1995, International Organization for Standardization, Geneva, CH, 1995, ISO 6708:1995. https://www.iso.org/standard/21274.html. (Last accessed on 18 January 2023).

[45] J. Haurum, T.B. Moeslund, Sewer-ML: A multi-label sewer defect classification dataset and benchmark, in: 2021 IEEE/CVF Conference on Computer Vision and Pattern Recognition, CVPR, IEEE Computer Society, Los Alamitos, CA, USA, 2021, pp. 13451–13462, http://dx.doi.org/10.1109/CVPR46437.2021.01325.

[46] J. Han, J. Pei, M. Kamber, Data Mining: Concepts and Techniques, Elsevier, 2011, http://dx.doi.org/10.1016/C2009-0-61819-5.